Exciton confinement and nonlocal nonlinear optical response of organic quantum wells

Ningjun Wang,* Jonathan K. Jenkins, Vladimir Chernyak,† and Shaul Mukamel
Department of Chemistry, University of Rochester, Rochester, New York 14627
(Received 19 January 1994)

The linear and nonlinear reflection spectra from a molecular quantum well with N layers are calculated using Green-function techniques. Exciton quantization in the direction normal to the lattice plane results in the appearance of discrete resonances in the linear reflection, with the same N-independent peak heights, and different superradiant linewidths. Nonlinear reflection measurements are ideal for probing states with a weak oscillator strength, provided their nonradiative damping is much smaller than the radiative decay rate. Size enhancement of $\chi^{(3)}$ due to dipole-dipole interaction and radiative coupling between layers is discussed.

I. INTRODUCTION

The study of the optical properties of multiple quantum-well (MQW) structures has largely focused on inorganic semiconductors.[1,2] However, interest in organic MQW nanostructures (also known as organic superlattices) has grown considerably recently in the light of modern methods for their fabrication.[3,4] The ability to grow defect-free samples on a mesoscopic scale is spurring a renewed interest in the theory of the optical properties of organic materials.[5] Both optical and electronic properties of organic structures are determined by the nature of excitons. The theory of excitons in molecular crystals and polymers was reviewed by Philpott.[6] In most organic crystals, excitons are believed to be of Frenkel or charge-transfer type,[7,8] although there are a few reports suggesting that excitons in anthracence crystals are of the Wannier type.[9,10] In recent experiments by Forrest and co-workers,[11,12] highly-ordered organic MQW structures have been grown using the ultrahigh-vacuum process of organic molecular-beam deposition. Optical-absorption and time-resolved photoluminescence measurements show an increased exciton energy (blueshift) and radiative decay rate with decreasing layer thickness from 100 to 10 Å.[11] These results are compatible with the strongly confined Wannier exciton model.[13,14] On the other hand, the oscillator strength observed in the absorption spectra of CuCl epitaxial films shows that the radiative decay rate decreases with decreasing well width.[15] This is the typical behavior of weakly confined Wannier excitons. Confined excitons have also been studied in other geometries such as molecular and atomic clusters.[16–18] The nonlinear optical response of confined excitons is also drawing considerable attention, since they show a size enhancement effect, which has potential device applications.[19] Spano and Mukamel predicted a crossover from $\sim N^2$ to $\sim N$ scaling of the nonlinear polarizability $\gamma^{(3)}$ of a linear aggregate as the aggregate size becomes comparable to the optical wavelength.[20] Ishihara and Cho have studied the nonlinear size enhancement for a multilayer structures.[21] Their model is essentially one dimensional since it does not include interactions between molecules in the same layer.

The solution of the Maxwell equations in a nonlocal medium is a well studied problem.[22,23] Since the external field creates several polariton modes in the medium, additional boundary conditions (ABC), on top of the Maxwell boundary conditions (MBC),[24] are needed to uniquely determine the relative amplitude of the various polariton modes. This "ABC" problem has been debated for a long time.[25–27] The ABC can be derived from a microscopic model of the medium including the details of the surface.[28,29] Another form of the microscopic solution to the ABC problem solves the nonlocal Maxwell equations without referring to the ABC.[30] Ishihara and Cho[21] used that approach to calculate the nonlinear response of a slab. In this procedure, one first calculates the nonlocal $\chi^{(1)}$ and $\chi^{(3)}$ microscopically and then substitutes them into the Maxwell equation to solve for the signal, using the MBC. $\chi^{(1)}$ and $\chi^{(3)}$ do not include radiative damping. However, it enters the signal through the Maxwell equations. The solution of the Maxwell equations with nonlocal $\chi^{(1)}$ and $\chi^{(3)}$ can usually only be found numerically, which makes it hard to clearly analyze the effects of the radiative damping on the signal. Moreover, the solution of the nonlocal Maxwell equations for nanostructures with complex geometries is not straightforward, since the MBC become quite complicated.

Recently, a new Green-function expression (GFE) for the linear and the nonlinear response of Frenkel exciton assemblies with arbitrary geometry was derived.[31] It fully takes into account the nonlocal properties of $\chi^{(3)}$ and the electric field, as well as radiative damping. Since it treats both the radiation field and the susceptibility microscopically, it completely avoids the use of MBC. Therefore, it is particularly useful for nanostructures with complex geometries. The signal is explicitly expressed in terms of Green functions that include radiative damping, which facilitates the analysis of its role. Applications to a two-dimensional molecular lattice (a monolayer) with nearest-neighbor interactions,[32] show an onresonant size enhancement of $\chi^{(3)}$ for small sizes.

In this paper, we apply the GFE to calculate the linear and nonlinear optical reflection spectra off a molecular

multilayer using the Frenkel exciton model. The present work generalizes our early study[32] to multilayers with N layers. Moreover, instead of using the nearest-neighbor interaction, we adopt a more realistic model, which takes into account the actual molecular charge distribution. We investigate the variation of exciton energy with the number of layers and with molecular size. We find that depending on the direction of the molecular transition dipole moment, the single-exciton energy can either increase or decrease with the number of layers. Like weakly confined Wannier excitons,[15] the exciton radiative decay rate decreases with decreasing well width. Due to the parity selection rule, only half of the exciton states are symmetric and contribute to the signal. We compare the linear reflection spectrum calculated from the GFE with that obtained from the solution of Maxwell equations in the long wavelength approximation (LWA), which holds only for thin layers. We further investigate the size enhancement of $\chi^{(3)}$ due to interaction and radiative coupling among different layers. The size enhancement depends on the ratio of the radiative and nonradiative decay rates.

II. GREEN-FUNCTION EXPRESSION (GFE) FOR REFLECTION SPECTRA

Consider a superlattice constructed out of identical monolayers, which are taken to be periodic two-dimensional square lattices in the x,y plane with lattice constant a. The distance between layers is a'. The polarization operator is given by[31,33]

$$\hat{\mathbf{P}}(\mathbf{r})=\sum_{m\lambda}\rho(\mathbf{r}-\mathbf{R}_{m\lambda})\hat{\mathbf{P}}_{m\lambda} , \tag{1}$$

$$\hat{\mathbf{P}}_{m\lambda}=\boldsymbol{\mu}(B_{m\lambda}+B^{+}_{m\lambda}) , \tag{2}$$

where $\mathbf{R}_{m\lambda}$ is the position of the mth molecule in the λth layer, and B^{+} and B are exciton creation and annihilation operators. The polarization density of each molecule $\rho(\mathbf{r})$ is assumed to have a two-dimensional Gaussian distribution form

$$\rho(\mathbf{r})=\frac{1}{\pi\sigma^2}\exp[-(r_x^2+r_y^2)/\sigma^2]\delta(r_z) , \tag{3}$$

with the normalization condition

$$\int d\mathbf{r}\,\rho(\mathbf{r})=1 . \tag{4}$$

This form mimics planar polycyclic aromatic organic molecules[12] with σ being the molecular size.

Invoking the rotating wave approximation, the linear polarization is[31]

$$\mathbf{P}^{(1)}_{n\lambda}(\omega)=-\sum_{m\alpha}\hat{G}_{n\lambda,m\alpha}(\omega)\boldsymbol{\mu}(\boldsymbol{\mu}\cdot\mathbf{E}^{\mathrm{ext}}_{m\alpha}) , \tag{5}$$

where $\mathbf{E}^{\mathrm{ext}}(\mathbf{r},\omega)$ is the external field and

$$\mathbf{E}^{\mathrm{ext}}_{m\mu}(\omega)\equiv\int d\mathbf{r}\,\mathbf{E}^{\mathrm{ext}}(\mathbf{r},\omega)\rho(\mathbf{r}-\mathbf{R}_{m\mu}) . \tag{6}$$

The single particle Green function $\hat{G}_{n\lambda,m\mu}(\omega)$ is defined by

$$\hat{G}_{n\lambda,m\mu}(\omega)=[\omega-H_{\mathrm{eff}}(\omega)+i\eta]^{-1}_{n\lambda,m\mu} , \tag{7}$$

where η is a small positive number which is set to $\eta=0$ at the end. Finite η can represent nonradiative damping.

The effective Hamiltonian matrix $H^{\mathrm{eff}}(\omega)$ is[32]

$$H^{\mathrm{eff}}_{n\lambda,m\mu}(\omega)=\Omega_0\delta_{mn}\delta_{\lambda\mu}+J_{n\lambda,m\mu}+\phi_{n\lambda,m\mu}(\omega) , \tag{8}$$

where $J_{n\lambda,m\mu}$ is the dipole-dipole interaction between molecules $n\lambda$ and $m\mu$

$$J_{n\lambda,m\mu}=\int d\mathbf{r}\int d\mathbf{r}'\rho(\mathbf{r}-\mathbf{R}_{n\lambda})\rho(\mathbf{r}'-\mathbf{R}_{m\mu})\boldsymbol{\mu}\cdot T(\mathbf{r}-\mathbf{r}')\cdot\boldsymbol{\mu} , \tag{9}$$

with the dipole-dipole interation tensor

$$T(\mathbf{r})=\frac{r^2-3\mathbf{r}\cdot\mathbf{r}}{r^5} . \tag{10}$$

$\phi_{n\lambda,m\mu}(\omega)$ is the material self-energy matrix[31,32] which contains all retardation effects,

$$\phi_{n\lambda,m\mu}(\omega)=\int d\mathbf{r}\int d\mathbf{r}'\rho(\mathbf{r}-\mathbf{R}_{n\lambda})\rho(\mathbf{r}'-\mathbf{R}_{m\mu})\times\boldsymbol{\mu}\cdot\mathcal{G}^{\perp}(\mathbf{r}-\mathbf{r}',\omega)\cdot\boldsymbol{\mu} , \tag{11}$$

where $\mathcal{G}^{\perp}$ is the Green function of the transverse electromagnetic field in vacuum

$$\mathcal{G}^{\perp}(\mathbf{r},\omega)=\int\frac{d^3q}{2\pi^2}\frac{\omega^2}{\omega^2-q^2c^2+i0}\left[1-\frac{\mathbf{qq}}{q^2}\right]\exp(i\mathbf{q}\cdot\mathbf{r})$$
$$=-\left[\left[\frac{\omega}{c}\right]^2+\nabla\nabla\right]\frac{\exp\left[i\frac{\omega}{c}r\right]}{r}+\nabla\nabla\frac{1}{r} . \tag{12}$$

In Eq. (8) Ω_0 is the bare molecular resonance frequency. The experimental isolated molecular resonance frequency Ω should include the self-Coulomb interaction $J_{n\lambda,n\lambda}$ and the Lamb shift $\mathrm{Re}\phi_{n\lambda,n\lambda}$, and is given by

$$\Omega\equiv\Omega_0+J_{n\lambda,n\lambda}+\mathrm{Re}\phi_{n\lambda,n\lambda} . \tag{13}$$

We have neglected the dependence of molecular resonance frequency Ω on the layer indices due to the excited state van der Waals interactions. These interactions may lead to the formation of surface states[34,35] resulting from the frequency change between surface and nonsurface molecules. They can be easily taken into account by replacing Ω with Ω_λ.

We shall decompose the $\mathbf{R}_{n\lambda}$ vector into $\mathbf{r}_n$ (parallel) and $\lambda a'\hat{\mathbf{z}}$ (normal) to the lattice plane,

$$\mathbf{R}_{n\lambda}=\mathbf{r}_n+\lambda a'\hat{\mathbf{z}} . \tag{14}$$

Due to the two-dimensional translational invariance in the plane, the Green function $G_{n\lambda,m\mu}$ depends on n and m only through $\mathbf{r}_n-\mathbf{r}_m$, and it can be recast in momentum space as

$$G_{\lambda\mu}(\mathbf{k},\omega)\equiv\sum_m G_{n\lambda,m\mu}\exp[-i\mathbf{k}\cdot(\mathbf{r}_n-\mathbf{r}_m)]$$
$$=[\omega-\Omega-J(\mathbf{k})-\phi(\mathbf{k},\omega)]^{-1}_{\lambda\mu} , \tag{15}$$

where $\mathbf{k}$ is a two-dimensional vector in the first Brillouin zone. The matrix elements $J_{\lambda\mu}(\mathbf{k})$ and $\phi_{\lambda\mu}(\mathbf{k},\omega)$ are the spatial Fourier transforms of $J_{n\lambda,m\mu}(1-\delta_{nm}\delta_{\lambda\mu})$ and $\phi_{n\lambda,m\mu}-\delta_{nm}\delta_{\lambda\mu}\mathrm{Re}\phi_{n\lambda,n\lambda}$ (with the self-Coulomb interactions and the Lamb shift excluded, see Appendix A),

$$J_{\lambda\mu}(\mathbf{k})+\phi_{\lambda\mu}(\mathbf{k},\omega)=\frac{2\pi i}{a^2}\sum_{b}\exp(i\sqrt{(\omega/c)^2-(\mathbf{k}+\mathbf{b})^2}|\lambda-\mu|a')$$
$$\times\left\{-\frac{(\omega/c)^2\mu^2-[\boldsymbol{\mu}^{\parallel}\cdot(\mathbf{k}+\mathbf{b})]^2}{\sqrt{(\omega/c)^2-(\mathbf{k}+\mathbf{b})^2}}+2\theta(\lambda-\mu)\boldsymbol{\mu}^{\parallel}\cdot(\mathbf{k}+\mathbf{b})\mu_z+\mu_z^2\sqrt{(\omega/c)^2-(\mathbf{k}+\mathbf{b})^2}\right\}$$
$$\times\rho(-\mathbf{k}-\mathbf{b})\rho(\mathbf{k}+\mathbf{b})-\delta_{\lambda\mu}(J_{n\lambda,n\lambda}+\mathrm{Re}\phi_{n\lambda,n\lambda}) , \tag{16}$$

where

$$\theta(\lambda-\mu)=\begin{cases}1, & \lambda>\mu\\ 0, & \lambda=\mu\\ -1, & \lambda<\mu ,\end{cases} \tag{17}$$

and $\rho(\mathbf{k})$ is the spatial Fourier transform of polarization density [Eq. (3)]

$$\rho(\mathbf{k})\equiv\int d\mathbf{r}\,\rho(\mathbf{r})\exp(-i\mathbf{k}\cdot\mathbf{r})=\exp\left[-\frac{k^2\sigma^2}{4}\right] . \tag{18}$$

Hereafter, we invoke the Markov approximation and set $\phi(\mathbf{k},\omega)\simeq\phi(\mathbf{k},\Omega)$. By doing so we replace the polariton dispersion by exciton dispersion.[36] For multilayers, this is a good approximation as long as k is not too close to ω/c, and N is not too large. Polariton effects are discussed in Appendix B.

In a stationary reflection experiment, the external field is

$$\mathbf{E}^{\mathrm{ext}}(\mathbf{r},t)=\mathbf{E}\exp[i(\boldsymbol{\kappa}\cdot\mathbf{r}-\omega t)]+\mathrm{c.c.} \tag{19}$$

Decomposing $\boldsymbol{\kappa}$ into $\mathbf{k}$ (parallel) and κ_z (normal) to the lattice plane,

$$\boldsymbol{\kappa}=\mathbf{k}+\kappa_z\hat{z} , \tag{20}$$

and following the procedure of reference,[32] we obtain the polarization with wave vector $\mathbf{k}$

$$\mathbf{P}_{n\lambda}(t)=\mathbf{P}_{\lambda}(\mathbf{k},\omega)\exp[i(\mathbf{k}\cdot\mathbf{r}_n-\omega t)] , \tag{21a}$$

$$\mathbf{P}_{\lambda}^{(1)}(\mathbf{k},\omega)=-\boldsymbol{\mu}(\boldsymbol{\mu}\cdot\mathbf{E})\rho(-\mathbf{k})\sum_{\mu=1}^{N}\hat{G}_{\lambda\mu}(\mathbf{k},\omega)\exp(i\kappa_z\mu a) , \tag{21b}$$

$$\mathbf{P}_{\lambda}^{(3)}(\mathbf{k},\omega)=-\tfrac{1}{2}\rho(-\mathbf{k})\rho(-\mathbf{k})\rho^*(-\mathbf{k})\sum_{\mu_1,\mu_2,\mu_3=1}^{N}\exp[i\kappa_z(\mu_1+\mu_2-\mu_3)a']\hat{R}^{(3)}_{\lambda,\mu_1,\mu_2,\mu_3}(\mathbf{k}\omega;\mathbf{k}\omega,\mathbb{k}\omega,-\mathbf{k}-\omega)\cdot\mathbf{EEE}^* . \tag{21c}$$

Here μ_1,μ_2,μ_3 are layer indices,

$$\hat{R}^{(3)}_{\lambda,\mu_1,\mu_2,\mu_3}(-\mathbf{k}-\omega;\mathbf{k}\omega,\mathbf{k}\omega,-\mathbf{k}-\omega)$$
$$=\mu\mu\mu\mu\sum_{\lambda',\lambda''=1}\hat{G}_{\lambda,\lambda'}(\mathbf{k},\omega)\hat{G}^*_{\lambda',\mu_3}(\mathbf{k},\omega)\hat{G}_{\lambda'',\mu_2}(\mathbf{k},\omega)$$
$$\times\hat{G}_{\lambda'',\mu_1}(\mathbf{k},\omega)\bar{\Gamma}_{\lambda',\lambda''}(2\mathbf{k},2\omega) , \tag{22}$$

and $\bar{\Gamma}_{\lambda'\lambda''}(2\mathbf{k},2\omega)$ is the two exciton scattering matrix

$$\bar{\Gamma}_{\lambda'\lambda''}(2\omega)=-2[F^{-1}(2\mathbf{k},2\omega)]_{\lambda'\lambda''} , \tag{23a}$$

$$F_{\lambda'\lambda''}(2\mathbf{k},2\omega)=\frac{ia^2}{(2\pi)^3}$$
$$\times\int_{1\mathrm{BZ}}d^2k'\int d\omega'\hat{G}_{\lambda'\lambda''}(\mathbf{k}',\omega')$$
$$\times\hat{G}_{\lambda'\lambda''}(2\mathbf{k}-\mathbf{k}',2\omega-\omega') . \tag{23b}$$

1BZ denotes an integration over the first Brillouin zone. These expressions are similar to those for the monolayer[32] except that here $\hat{G},\bar{\Gamma}$, and F are $N\times N$ matrices.

Using the external field Eq. (19), we calculate in Appendix C the reflected field amplitude $E_r(\omega)$ (with wave vector $\boldsymbol{\kappa}'=\mathbf{k}-\kappa_z\hat{z}$) and the transmitted field $E_t(\omega)$ (with wave vector $\boldsymbol{\kappa}$)

$$\mathbf{E}_r(\omega)=\frac{2\pi i(\omega/c)^2}{a^2\sqrt{(\omega/c)^2-k^2}}\rho(\mathbf{k})$$
$$\times\sum_{\lambda=1}^{N}(1-\hat{\kappa}'\hat{\kappa}')\cdot\mathbf{P}_{\lambda}(\mathbf{k},\omega)e^{i\kappa_z\lambda a'} , \tag{24}$$

$$\mathbf{E}_t(\omega)=\mathbf{E}+\frac{2\pi i(\omega/c)^2}{a^2\sqrt{(\omega/c)^2-k^2}}\rho(\mathbf{k})$$
$$\times\sum_{\lambda=1}^{N}(1-\hat{\kappa}\hat{\kappa})\cdot\mathbf{P}_{\lambda}(\mathbf{k},\omega)e^{-i\kappa_z\lambda a'} . \tag{25}$$

The linear and nonlinear reflection coefficients, $S_{\mathrm{LR}}(\omega)$ and $S_{\mathrm{NR}}(\omega)$, are finally given by

$$|E_r(\omega)|^2\equiv S_{\mathrm{LR}}(\omega)|E|^2+S_{\mathrm{NR}}(\omega)|E|^4+O(E^6) , \tag{26}$$

where

$$S_{\mathrm{LR}}(\omega)=|E_r^{(1)}(\omega)|^2/|E|^2=\frac{4\pi^2(\omega/c)^4}{a^4[(\omega/c)^2-k^2]}|\rho(\mathbf{k})\rho(-\mathbf{k})|^2[\mu^2-(\boldsymbol{\mu}\cdot\hat{\kappa}')^2](\boldsymbol{\mu}\cdot\hat{E})^2$$
$$\times\left|\sum_{\lambda\mu=1}^{N}\hat{G}_{\lambda\mu}(\mathbf{k},\omega)\exp[i\kappa_z(\lambda+\mu)a']\right|^2 , \tag{27}$$

and

$$S_{\rm NR}(\omega)=2\,{\rm Re}\{[E_r^{(1)}(\omega)]^* E_r^{(3)}(\omega)\}/|E|^4 \propto {\rm Re}\Bigg\{\sum_{\lambda_1\lambda_2=1}^{N}\hat{G}^*_{\lambda_1\lambda_2}(\mathbf{k},\omega)\exp[-i\kappa_z(\lambda_1+\lambda_2)a']$$
$$\times\sum_{\lambda,\mu_1,\mu_2,\mu_3,\lambda',\lambda''=1}^{N}\exp[i\kappa_z(\lambda+\mu_1+\mu_2-\mu_3)a']$$
$$\times\hat{G}_{\lambda,\lambda'}(\mathbf{k},\omega)\hat{G}^*_{\lambda',\mu_3}(\mathbf{k},\omega)\hat{G}_{\lambda'',\mu_2}(\mathbf{k},\omega)$$
$$\times\hat{G}_{\lambda'',\mu_1}(\mathbf{k},\omega)\bar{\Gamma}_{\lambda',\lambda''}(2\mathbf{k},2\omega)\Bigg\}\,. \tag{28}$$

Here $E_r^{(j)}(\omega), j=1,3$ denotes the reflected field $E_r(\omega)$ to jth order with respect to $E^{\rm ext}$. It can be obtained by substituting Eqs. (21b) and (21c) into Eq. (24).

As a check, we note that energy conservation to linear order of $E^{\rm ext}$ implies

$$|E|^2=|E_r^{(1)}|^2+|E_t^{(1)}|^2\,. \tag{29}$$

In Appendix C we show that this relation indeed holds for a monolayer ($N=1$). Our numerical results satisfy this relation for multilayers as well.

III. THE LINEAR REFLECTION SPECTRUM

We present numerical calculations for an in-plane transition dipole oriented 45° with respect to the x and y axes, i.e., $\boldsymbol{\mu}=(\hat{x}+\hat{y})\mu/\sqrt{2}$. We further set $a=a'$, $\sigma=0.1a$, the optical wavelength $\bar{\lambda}\equiv 2\pi c/\Omega=1000a$, and assume normal incidence ($\boldsymbol{\kappa}$ along z) and $\mathbf{E}\|\boldsymbol{\mu}$. We further neglect nonradiative damping, so that $\eta\to+0$. We have set $\hbar=1$, and use $W\equiv\mu^2/a^3$ as the unit of energy and frequency. The linear reflection spectra are shown in Fig. 1 (for 1–4 layers), and Fig. 2 (for 5, 10, and 20 layers). The resonance frequencies are redshifted with respect to the isolated molecule, which is due to the attractive in-plane nearest-neighbor interaction. When the multilayer thickness is much smaller than the optical wavelength ($Na\ll\bar{\lambda}$), we observe $N^*/2$ peaks where $N^*\equiv N$ for even N and $N^*\equiv N+1$ for odd N; all of these peaks have the same height, which is independent of N. The highest frequency resonance has the maximum cooperative radiative width, and it shifts to the blue as N is increased.

The discrete resonances in the linear reflection spectrum are related to the formation of polariton modes in the multilayers. The polariton dispersion in a molecular superlattice was previously studied by Agranovich and Kravtsov[37] and Knoester.[36] In order to interpret our numerical results, we derive an approximate analytic expression for the linear reflection spectrum. We denote the real and the imaginary parts of the intermolecular interaction $J+\phi$ by $\tilde{J}$ and $-\Gamma$, respectively,

$$J_{\lambda\mu}(\mathbf{k})+\phi_{\lambda\mu}(\mathbf{k},\Omega)\equiv\tilde{J}_{\lambda\mu}(\mathbf{k})-i\Gamma_{\lambda\mu}(\mathbf{k})\,. \tag{30}$$

$\tilde{J}_{\lambda\mu}$ is the effective dipole-dipole interaction and $\Gamma_{\lambda\mu}$ is the radiative decay matrix. Since $\mu_z=0$ and a is much smaller than the optical wavelength, i.e.,

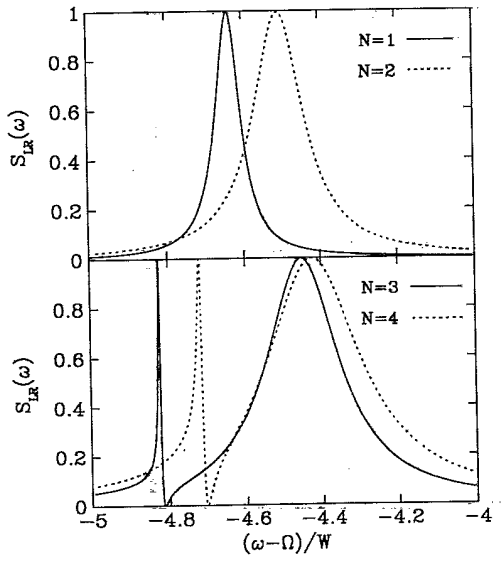

FIG. 1. Linear reflection spectrum of molecular multilayers with in-plane dipole moment $\mu(\hat{x}+\hat{y})/\sqrt{2}$ and normal incidence, with 1–4 layers. Nonradiative decay rate $\eta=0$.

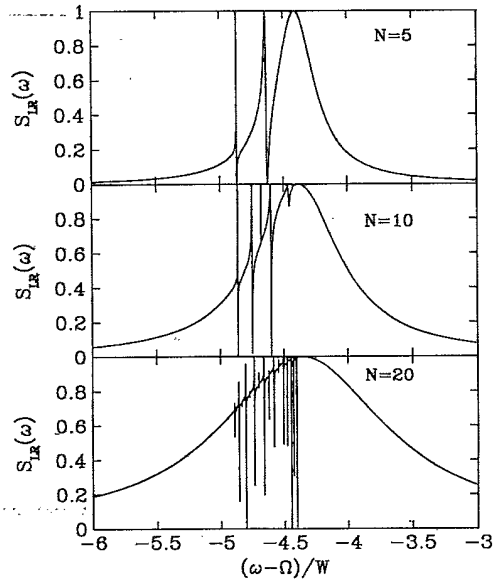

FIG. 2. Same as in Fig. 1 but for 5, 10, and 20 layers, as indicated.

$|\mathbf{b}| \simeq 2\pi/a \gg \Omega/c$, only the $\mathbf{b}=0$ term in Eq. (16) contributes to $\Gamma_{\lambda\mu}(\mathbf{k})$. This term depends only weakly on λ and μ, as long as the multilayer thickness Na is much smaller than the optical wavelength. We thus assume that $\Gamma_{\lambda\mu}(\mathbf{k}=0)$ to be independent of λ and μ,

$$\Gamma_{\lambda\mu}(\mathbf{k}=0)=\Gamma=2\pi\mu^2\Omega/(a^2c) . \tag{31}$$

The $\mathbf{b}\neq 0$ terms vanish exponentially with interlayer distance $\sim\exp(-|\lambda-\mu|\cdot|\mathbf{b}|a)$. Their sum is real and is much larger than the real part of the $\mathbf{b}=0$ term. Therefore, $\tilde{J}_{\lambda\mu}(\mathbf{k})$ decrease rapidly with $|\lambda-\mu|$ and may be neglected for $|\lambda-\mu|>1$, setting

$$\tilde{J}_{\lambda\mu}(\mathbf{k}=0)=J_0\delta_{\lambda\mu}+J_1(\delta_{\lambda,\mu+1}+\delta_{\lambda,\mu-1}), \tag{32}$$

where J_0 and J_1 denote the in-plane and interplane interactions, respectively. Using these approximate forms of $\tilde{J}_{\lambda\mu}$ and $\Gamma_{\lambda\mu}$, and further setting $\exp[i\kappa_z(\lambda+\mu)a]\simeq 1$, we can calculate the linear signal analytically (see Appendix D),

$$S_{\mathrm{LR}} \propto \left| \sum_{\lambda,\mu=1}^{N} \hat{G}_{\lambda\mu}(\mathbf{k}=0,\omega) \right|^2 = \left| \frac{\sum_{\alpha=1}^{N} \xi_\alpha/[\omega-\varepsilon_\alpha+i\eta]}{1+i\Gamma\sum_{\alpha=1}^{N} \xi_\alpha/[\omega-\varepsilon_\alpha+i\eta]} \right|^2 , \tag{33}$$

where ε_α are the eigenvalues of the real symmetric matrix $\tilde{J}_{\lambda\mu}(\mathbf{k}=0)$, which represent the energies of the αth exciton eigenstate with zero in-plane momentum and in the absence of radiative damping,

$$\varepsilon_\alpha=\Omega+J_0+2J_1\cos[\alpha\pi/(N+1)], \alpha=1,\ldots,N . \tag{34}$$

ξ_α is proportional to the oscillator strength of the αth exciton eigenstate

$$\xi_\alpha \equiv \left| \sum_{\mu=1}^{N} \psi_\alpha(\mu) \right|^2 = \frac{2}{N+1}\sin^2(\alpha\pi/2)\cot^2[\alpha\pi/(2N+2)] , \tag{35}$$

where $\psi_\alpha(\mu)$ [Eq. (D8)] is the wave function of the αth exciton eigenstate. From Eq. (35) we see that the oscillator strength vanishes ($\xi_\alpha=0$) for even values of α, which, therefore, do not contribute to the signal.[15] This can be easily rationalized since eigenstates are either symmetric (odd α) or antisymmetric (even α) in the z direction around the center of the slab. Assuming that the exciton energies ε_α are well separated, we see from Eq. (33) that in the vicinity of a particular resonance, i.e., when $\omega\rightarrow\varepsilon_\alpha$, $\alpha=1,3,\ldots,N^*-1$,

$$S_{\mathrm{LR}} \propto \frac{\xi_\alpha^2}{(\omega-\varepsilon_\alpha)^2+(\gamma_\alpha+\eta)^2} , \tag{36}$$

where γ_α represents the radiative exciton width,

$$\gamma_\alpha=\Gamma\xi_\alpha=\frac{2\Gamma}{N+1}\cot^2[\alpha\pi/(2N+2)]\sin^2(\alpha\pi/2) . \tag{37}$$

Therefore, when the nonradiative width vanishes ($\eta=0$), there are $N^*/2$ peaks, all with the same height $1/\Gamma^2$ which is independent of N, and with the radiative width $\Gamma\xi_\alpha$ proportional to the oscillator strength. We have from Eq. (35) for $\alpha \ll N$

$$\xi_\alpha \sim \frac{N}{\alpha^2} , \tag{38}$$

which agrees with Ref. 15. The $\alpha=1$ state carries most of the oscillator strength, and its radiative decay rate is proportional to N, which implies cooperativity (superradiance); all other α states have a much weaker oscillator strength. This liner scaling with N of the radiative width breaks down when Na is comparable to the optical wavelength, because Eq. (31) no longer holds. Knoester[36] showed that for $Na>\bar{\lambda}$, the decay rate shows an oscillatory dependence on Na, and its amplitude drops off as $1/(Na)$.

We next discuss the size dependence of the resonance peak. When Na is much smaller than the optical wavelength and in the absence of interaction and radiative coupling between planes, the linear reflection signal is proportional to N^2

$$S_{\mathrm{LR}} \propto \frac{N^2}{(\omega-\Omega-J_0)^2+(\eta+\Gamma)^2} . \tag{39}$$

This may be easily rationalized, since the fields reflected from different planes are in phase, provided the distance between planes is much smaller than the optical wavelength.

When Coulomb interaction and radiative coupling between different layers are incorporated, we see from Eq. (36) that the $\alpha=1$ state, which carries most of the oscillator strength, has the highest resonance peak. When η is much smaller than the radiative width of the $\alpha=1$ state, the peak magnitude at $\omega=\varepsilon_1$, $1/\Gamma^2$, is independent of N, and the $\sim N^2$ dependence is lost. This is due to the increased radiative width with N, induced by interplane radiative coupling. When η is much larger than the radiative width of the $\alpha=1$ state, the $\alpha=1$ peak is given by $4\eta^{-2}\cot^4[\pi/(2N+2)]\cdot(N+1)^{-2}$, and the N^2 dependence is retained for large N. In this case, the interplane interaction is still present, but the effects of interplane radiative coupling are suppressed by the nonradiative width which dominates the radiative width. Therefore, the interplane interaction does not reduce the size enhancement of the linear signal, whereas the interplane radiative coupling does.

For our geometry, the in-plane molecular interaction is attractive ($J_0<0$), and the neighboring plane molecular interaction is repulsive ($J_1>0$). Since in our calculation, J_0 is much larger than J_1, the spectrum is redshifted with respect to the isolated molecule. We further see from Eq. (34) that the superradiant ($\alpha=1$) state is the highest-frequency peak, and it shifts to the blue as the number of layers N is increased. For μ perpendicular to the plane, the neighboring plane molecular interaction is attractive, and the superradiant state is the lowest-frequency peak. It then shifts to red as the number of layers N is increased. Therefore, whether the exciton energies increase

or decrease with layer thickness is determined by the sign of the interplane interaction (J_1), which is related to the direction of the molecular transition dipole moment. In semiconductors, the exciton energy usually increases as the layer thickness decreases, since the effective electron and hole mass is usually positive. In contrast with molecular crystals, the semiconductor band structure is not determined by the dipole-dipole interaction and the sign of the effective (electron and hole) mass does not change with the direction of the transition dipole moment.

Denoting the resonance frequency of the superradiant $\alpha=1$ state by ω_0, we have calculated its frequency shift $\omega_0-\Omega$ with respect to isolated molecule frequency Ω as a function of molecular size σ (note that both ω_0 and Ω depend on σ). Figure 3 shows that the shift increases with σ. This is to be expected since the frequency shift is mainly due to the in-plane molecular interactions which become stronger with larger molecular size.

We next compare our results with the solution of the Maxwell equations in the LWA, where we treat the slab as a continuous medium with the linear susceptibility

$$\chi^{(1)}(\mathbf{r},\mathbf{r}',\omega)=\bar{\chi}^{(1)}(\omega)\delta(\mathbf{r}-\mathbf{r}') \ . \tag{40}$$

Here $\bar{\chi}^{(1)}(\omega)$ is the position averaged linear susceptibility. From Eq. (21b) we have

$$\bar{\chi}^{(1)}(\omega)=-\frac{\mu^2}{a^3 N}\sum_{\lambda,\mu=1}^{N} G_{\lambda\mu}(\mathbf{k}=0) \ , \tag{41}$$

and $G_{\lambda\mu}(\mathbf{k}=0)$ is the Green function without retardation effects[31]

$$G_{\lambda\mu}(\mathbf{k}=0)\equiv[\omega-\Omega-J(\mathbf{k}=0)+i\eta]^{-1} \ . \tag{42}$$

We can then solve the Maxwell equation inside and outside the slab, and use the Maxwell boundary conditions (the electric field parallel to the interface and the electric displacement D normal to the interface are continuous) (Ref. 24) to match them. The linear reflection spectrum for normal incidence is then

$$S^{M}_{\mathrm{LR}}(\omega)=\left|\frac{(k^2-k'^2)[1-\exp(2ik'Na)]}{(k+k')^2-(k-k')^2\exp(2ik'Na)}\right|^2 , \tag{43}$$

where κ' is the complex optical wave vector inside the slab

$$\kappa'\simeq(\Omega/c)\sqrt{\epsilon(\omega)} \ , \qquad \epsilon(\omega)=1+4\pi\bar{\chi}^{(1)}(\omega) \ . \tag{44}$$

Numerical calculations verify that $S^{M}_{\mathrm{LR}}(\omega)$ is identical with the GFE result for small N. Figure 4 shows that for $\eta=0.004W$, $S^{M}_{\mathrm{LR}}(\omega)$ begins to deviate from the GFE result near the highest-frequency peak at $N=11$. The deviation is due to the breakdown of LWA when Na is comparable to the optical wavelength, $2\pi/k'$, inside the medium. k' reaches its maximum when ω is resonant with the exciton state with the largest oscillator strength (highest-frequency peak). This explains why the deviation is largest for ω near the highest-frequency peak, where $2\pi/k'$ is the shortest. The maximum k' is proportional to $\eta^{-1/2}$, and we expect $S^{M}_{\mathrm{LR}}(\omega)$ to hold for larger values of N as η increases. This is verified by our numerical calculations as well.

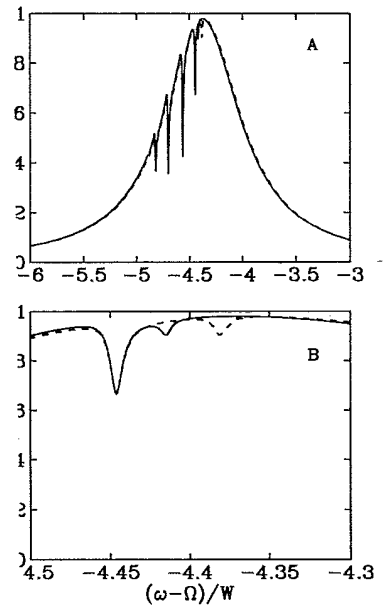

FIG. 4. (a) Linear reflection spectrum for $N=11$ and nonradiative damping $\eta=0.004W$. Solid line is the GFE result, and dashed line is the result of the LWA Eq. (43). (b) The same calculation shown on an expanded scale.

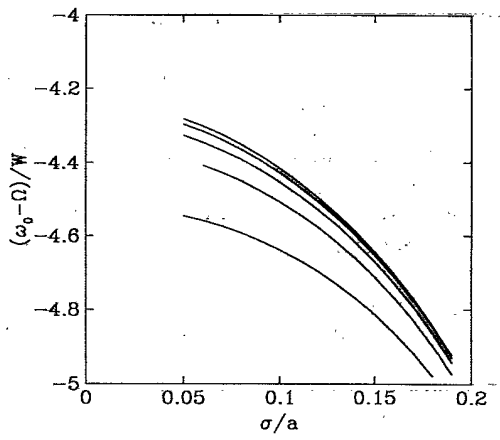

FIG. 3. The spectral shift $\omega_0-\Omega$ of the resonance frequency of the superradiant state (ω_0), i.e., the state with the strongest oscillator strength, with respect to isolated molecule Ω as a function of molecular size σ with in-plane transition dipole moment $\mu(\hat{x}+\hat{y})/\sqrt{2}$ and normal incidence. The number of layers from bottom to the top is 1, 2, 3, 4, and 5.

IV. THE NONLINEAR REFLECTION SPECTRUM

In Fig. 5, we display the nonlinear reflection spectrum (solid line) calculated using Eq. (28) for the same geometry as in Sec. III, and in the absence of nonradiative damping $\eta=0$. Note that for one and two layers, the

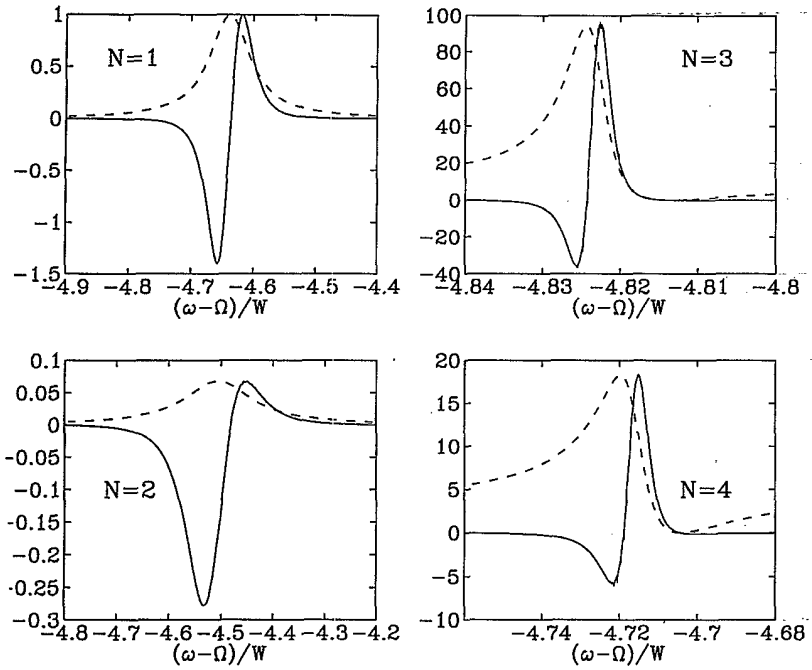

FIG. 5. Comparison of the nonlinear reflection spectrum $S_{NR}(\omega)$ (solid) with the linear reflection spectrum $S_{LR}(\omega)$ (dashed). The vertical scale shows the relative magnitude of $S_{NR}(\omega)$. $S_{LR}(\omega)$ is normalized to have the same height as $S_{NR}(\omega)$.

resonance frequency of the nonlinear signal coincides with that of the linear reflection signal (dashed line), whereas for three and four layers, it coincides with the red peak ($\omega \simeq \varepsilon_3$) of the linear reflection. Therefore, the main contribution to the nonlinear signal for three and four layers is from the ε_3 state, which has a much smaller radiative width than the superradiant state ε_1. The smaller the oscillator strength, the larger the peak magnitude. Note that for three (four) layers, there are one (two) antisymmetric states with a very small (but finite) radiative width. These states should contribute a sharp peak to the nonlinear reflection spectrum when $\eta=0$. They are outside the frequency range of Fig. 5. When the nonradiative damping η is much larger than the radiative width of antisymmetry states, they make a negligible contribution to the nonlinear signal.

Figure 5 also shows that the peak magnitude of the nonlinear reflection signal for an odd number of layers is larger than that of the closest even number of layers, and both increase with the number of layers. This is due to the radiative coupling between layers.

In order to rationalize these results, we use the local-field approximation (LFA) (Ref. 32)

$$\bar{\Gamma}_{\lambda'\lambda''}(2\mathbf{k},2\omega) = -4(\omega-\Omega)\delta_{\lambda'\lambda''} , \tag{45}$$

and Eqs. (31) and (32). For $Na \ll \bar{\lambda}$, we show in Appendix D that when $\omega \simeq \varepsilon_\alpha$, $\alpha = 1,3,\ldots,N^*-1$, the resonant nonlinear signal is

$$S_{NR}(\omega) \propto A_\alpha(\gamma_\alpha+\eta)^5 \frac{\omega-\varepsilon_\alpha}{|\omega-\varepsilon_\alpha+i(\gamma_\alpha+\eta)|^6} , \tag{46}$$

$$A_\alpha = -\frac{(3+\delta_{2\alpha,N+1})(\varepsilon_\alpha-\Omega)}{\Gamma^3} \frac{2\gamma_\alpha^3}{(N+1)(\gamma_\alpha+\eta)^5} . \tag{47}$$

The width of the positive (as well as) the negative peak in the nonlinear reflection spectrum is $\gamma_\alpha+\eta$. The peak height is proportional to A_α for odd α. The even α states carry no oscillator strength and make no contribution to the nonlinear signal. $S_{NR}(\omega)$ [Eq. (46)] for $N=6$ and $\eta=0$ is displayed in Fig. 6.

Equation (46) is not identical to the GFE result with full dipole-dipole interaction; nevertheless it provides a good physical insight on the size enhancement. Equation (46) shows that the resonance frequencies of the nonlinear reflection signal $\varepsilon_\alpha \pm (\gamma_\alpha+\eta)/\sqrt{5}$ are close to those of the linear reflection signal (i.e., at the single-exciton energies ε_α). From Eq. (47) we clearly see that when the nonradiative width is much smaller than the smallest radiative width of symmetric states $\eta \ll \gamma_{N^*-1}$, we have

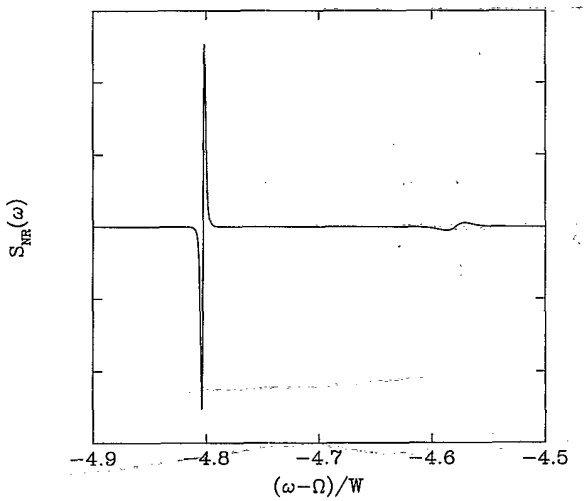

FIG. 6. Nonlinear reflection spectrum for six layers in the LFA and nearest-neighbor interplane interaction Eq. (46). Nonradiative damping $\eta=0$.

$A_\alpha \sim \gamma_\alpha^{-2}$. Therefore, states with a smaller oscillator strength produce stronger distinct resonance peaks (see Fig. 6). The superradiant state that carries most of the oscillator strength makes a negligible contribution to the nonlinear signal. The nonlinear reflection experiment is ideal for probing states with a weak oscillator strength, since the broad background due to superradiant states which dominates the linear reflection spectrum is absent.

In the opposite limit, when the nonradiative width is much larger than the largest radiative width $\eta \gg \gamma_1$, then $A_\alpha \sim \gamma_\alpha^3$ and the superradiant state dominate the nonlinear spectrum. When $\gamma_{N^*-1} \ll \eta \ll \gamma_1$, the state whose radiative width is equal to $3\eta/2$ (comparable radiative and nonradiative width) has the strongest peak. In the absence of interaction and radiative coupling between different layers and $Na \ll \bar{\lambda}$, the nonlinear reflection signal should scale as N^2,

$$S_{\rm NR}(\omega) \propto -4N^2 \frac{[\omega-\Omega-J_0(\mathbf{k})](\omega-\Omega)}{|\omega-\Omega-J_0(\mathbf{k})+i(\Gamma+\eta)|^6} . \quad (48)$$

We next consider the size enhancement due to the interaction and radiative coupling between layers. Since size enhancement strongly depends on the relative magnitudes of the nonradiative and the radiative damping, we will examine the following limiting cases.

(i) We first assume that the nonradiative damping is much smaller than the smallest radiative width, i.e.,

$$\eta \ll \gamma_{N^*-1} = \frac{2\Gamma}{N+1} \tan^2[O_N \pi/(2N+2)] ,$$

where $O_N=2$ for even N and $O_N=1$ for odd N. As discussed above, the strongest peak is near $\omega=\varepsilon_{N^*-1}$, with peak magnitude A_{N^*-1}. For $N \gg 1$,

$$A_{N^*-1} \sim N^5/O_N^4 . \quad (49)$$

Due to the O_N factor, the peak magnitude of even N is smaller than that of the closest odd N. Compared to the $\sim N^2$ dependence of Eq. (48), we see a clear size enhancement due to interplane coupling. The interaction J between layers results in a discrete set of exciton energies, and the radiative coupling causes the redistribution of radiative width among different states. The size enhancement is due to the decrease of radiative width γ_{N^*-1}. A_{N^*-1} increases with N and reaches its maximum when the radiative width is comparable to the nonradiative width $\gamma_{N^*-1}=3\eta/2$. The optimal number of layers that has maximum peak magnitude N_m (it is odd) can be determined by the condition $\gamma_{N_m}=3\eta/2$, which yields

$$N_m \simeq \left[\frac{\Gamma\pi^2}{3\eta}\right]^{1/3} . \quad (50)$$

This is shown in Fig. 7, which displays the lowest-frequency peak height A_{N^*-1} as a function of the number of layers Eq. (47). For even N the peak height is lower than for odd N. As η increases, the peak height decreases as well as N_m.

(ii) We next assume that the nonradiative width is much larger than the largest radiative width, i.e.,

$$\eta \gg \gamma_1 = \frac{2\Gamma}{N+1} \cot^2[\pi/(2N+2)] .$$

The superradiant state $\alpha=1$ now has the largest peak magnitude,

$$A_1 = -\frac{16(\varepsilon_1-\Omega)(3+\delta_{N,1})}{(N+1)^4\eta^5} \cot^6[\pi/(2N+2)] , \quad (51)$$

with $A_1 \sim N^2$ for $N \gg 1$ but still much smaller than $\bar{\lambda}/a$. There is no size enhancement due to the interplane coupling in this case, since the nonradiative width dominates the radiative width, and the redistribution of radiative width due to the interplane radiative coupling has a negligible effect on the signal.

(iii) When the nonradiative damping is in between the smallest and the largest radiative widths, i.e.,

$$\frac{2\Gamma}{N+1} \tan^2[O_N \pi/(2N+2)] \ll \gamma_1 \ll \frac{2\Gamma}{N+1} \cot^2[\pi/(2N+2)] ,$$

the state whose radiative width $\gamma_\alpha \simeq 3\eta/2$ has the largest peak magnitude, which decreases as $1/(N+1)$.

We have shown in case (i) that the additional size enhancement is due to the decreased radiative width, which is caused by both the interplane interaction and radiative coupling. In case (ii), where the radiative width is suppressed by the nonradiative width, there is no size enhancement despite the interplane interaction. Neglecting the interplane interaction but retaining interplane radiative coupling, setting $\varepsilon_\alpha=\Omega+\tilde{J}_0(\mathbf{k})$ in Eq. (D11) in Appendix D and substituting into Eq. (D9), we have

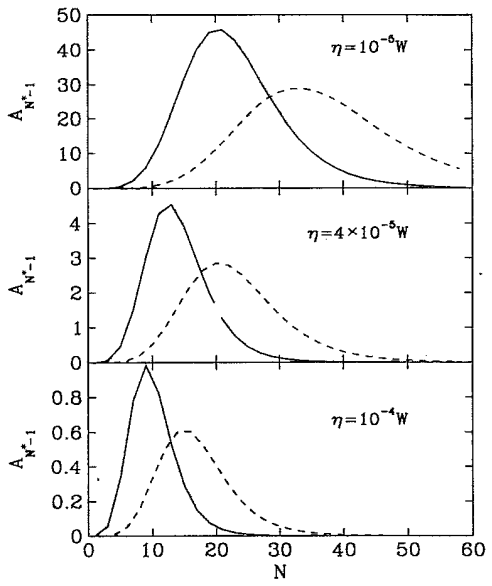

FIG. 7. The lowest-frequency peak height in the nonlinear reflection spectrum A_{N^*-1} [Eq. (47)] versus the number of layers for various values of the nonradiative decay rate η. Solid (dashed) line correspond to odd (even) values of N. The vertical scale shows their relative magnitudes.

$$S_{\rm NR}(\omega)=-\frac{4N^2[\omega-\Omega-J_0(\mathbf{k})](\omega-\Omega)}{|\omega-\Omega-J_0(\mathbf{k})+i(N\Gamma+\eta)|^6}\ , \qquad (52)$$

and the enhancement effect of case (i) is lost. In this case, all exciton states have the same energies and it is impossible to optically select the state with the smallest radiative width. Therefore, interplane radiative coupling alone does not produce the additional size enhancement either. It can be attributed to the combination of interplane interaction and radiative coupling.

In the above analysis, we have used the LFA and neglected the enhancement in the two exciton scattering matrix $\bar{\Gamma}$. The effect of $\bar{\Gamma}$ will be discussed below. We have previously shown that for d dimensional lattices with periodic boundary conditions, $\bar{\Gamma}$ is proportional to N in the small size limit, and becomes independent of N when the size is large.[32] A similar analysis was given in Ref. 20. The reason is as follows: when the lattice size is small, the exciton eigenstates are discrete, and are delocalized due to interaction among molecules. When the frequency of the external field ω is resonant with a particular delocalized exciton state, the system is excited to that state, which results in a size enhancement in $\bar{\Gamma}$ due to the induced phase coherence between different sites. When the lattice is large, the exciton eigenstates become so close that the laser creates many exciton states. The phase coherence among different sites is cancelled due to interference among different exciton states, and the size enhancement is destroyed. An alternative way of analyzing the size enhancement effect is by expressing $\chi^{(3)}$ in terms of single-exciton and two-exciton global eigenstates of the entire sample. The contributions to $\chi^{(3)}$ from single-photon and two-photon resonance have opposite sign and are proportional to N and $N-1$, respectively. For small sizes, the resonance frequencies of these two contributions are well separated and it is possible to tune the laser frequency to select one contribution, and thus $\chi^{(3)}\sim N$. For large sizes, resonance frequencies from these two contributions are very close, and $\chi^{(3)}$ becomes independent of N due to the interference of the two contributions.[20]

V. CONCLUSION AND DISCUSSION

In a previous paper,[32] we predicted a new peak in the nonlinear reflection spectrum of a molecular monolayer with nearest-neighbor interactions (see the upper panel of Fig. 8). This peak does not show up for dipole-dipole interactions. This can be understood as follow: The additional peak is caused by the sharp edge of the two-exciton density of states with zero center-of-mass momentum (for a monolayer, it coincides with the total single-exciton density of states). Figure 9 shows that the total single-exciton density of states for dipole-dipole interactions has a much more gradual edge (at the lower band edge) compared with the nearest-neighbor interaction, and consequently, it does not create the additional peak.

In this paper, we have calculated the linear and nonlinear reflection spectra from a molecular multilayers. When the layer thickness is much smaller than $\bar{\lambda}$, we find $N^*/2$ resonances related to the discrete exciton eigenstates induced by confinement in the z direction. Due to the parity selection rule, half of the states are antisymmetric in the z direction, carry no oscillator strength, and make no contribution to the optical signal. The exciton energies may shift to the blue or to the red as the layer thickness decreases, depending on the direction of the transition dipole moment, while in semiconductors they are usually blueshifted regardless of the direction of transition dipole moment. One of the exciton states carries most of the oscillator strength which is proportional to the number of layers (superradiance). This is reminiscent of Wannier excitons in the weak confinement limit, but

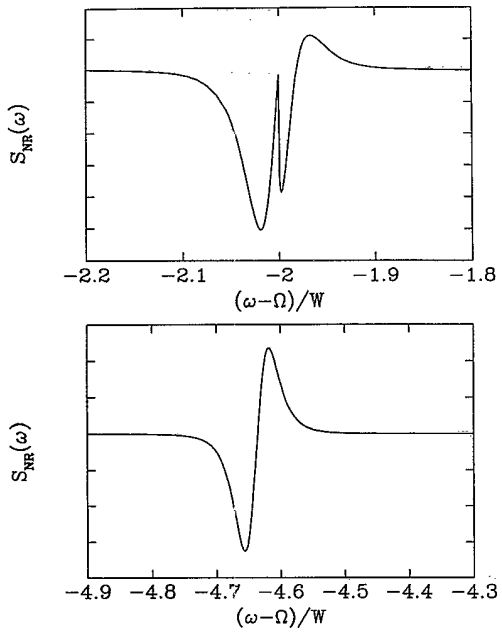

FIG. 8. Nonlinear reflection from a molecular monolayer with nearest-neighbor in-plane interactions (upper panel), and with the full dipole-dipole interaction (lower panel).

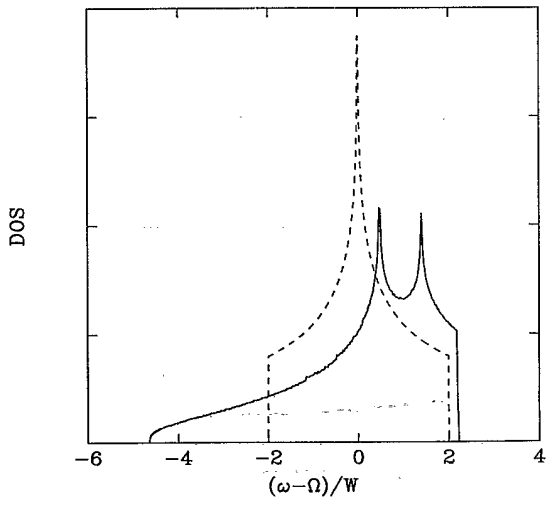

FIG. 9. Total single-exciton density of states of a molecular monolayer with dipole-dipole interactions and in-plane transition dipole moment $\mu(\hat{x}+\hat{y})/\sqrt{2}$ (solid line), and with nearest-neighbor in-plane interactions (dashed line).

not in the strong confinement limit. The LWA applies when the layer thickness is much smaller than the optical wavelength inside the multilayers.

For the nonlinear reflection spectrum, the states whose radiative width is comparable to the nonradiative width show the strongest resonances. The nonlinear reflection spectrum is ideal for probing states with a relatively weak oscillator strength provided the nonradiative width is small, since there is no broad background peak due to the superradiance state, which dominates the linear reflection spectrum. The optimal number of layers that has the largest peak magnitude is proportional to $\eta^{-1/3}$. In our analysis, we have assumed the multilayers thickness to be small compared with the optical wavelength. However, the GFE results of Eqs. (27) and (28) are valid for an arbitrary thickness.

We have shown that in the linear reflection, the interplane radiative coupling suppresses the size enhancement of the superradiant state by increasing its radiative width. In the nonlinear reflection, $S_{\rm NR}\sim G^*GG^*GG\overline{\Gamma}$, there are two sources of enhancement: (1) The enhancement coming from the five G factor when the nonradiative damping is much smaller than the smallest radiative damping. This enhancement is due to the decrease of radiative width caused by the combination of interplane interaction and radiative coupling. (2) The enhancement of the $\overline{\Gamma}$ factor, which is due to the energy splitting of two exciton states caused by interplane interaction.

The discrete resonances in the linear and the nonlinear reflection spectrum can be observed only when their average spacing $8\mu^2/(a^3N)$ is larger than their linewidth γ_T. For anthracene, $\mu=0.61\ e$ Å (e is the electron charge), $a\simeq 8$ Å.[38] The linewidth of the 0-0 transition varies from 0.01 $\rm cm^{-1}$ at temperature 4.2 K to 10 $\rm cm^{-1}$ at temperature 80 K.[39] Taking $\gamma_T=10\ \rm cm^{-1}$, one should be able to observe these resonances in nonlinear reflection in systems with up to 60 layers. In linear reflection spectrum, Fig. 2 shows that the discrete resonances can be observed up to only 20 layers due to superradiance. We thus expect these resonances to be observable in multilayers of aromatic molecules such as perylenetetracarboxylic dianhydride.[3,11] Recently such resonances were observed in CuCl quantum wells.[15] This is a weakly confined Wannier exciton system which can be described using the Frenkel exciton model.[40] In this system for thickness of 157 Å, the spacing between $n=1$ and $n=3$ resonances is approximately equal to their linewidth, 5 meV (estimated from Fig. 1 of Ref. 15).

ACKNOWLEDGMENTS

The support of the National Science Foundation and the Air Force Office of Scientific Research is gratefully acknowledged. We thank Dr. Loys Belleguie and the Restricted Geometries Group at the NSF Center for Photoinduced Charge Transfer for useful comments.

APPENDIX A: DERIVATION OF EQ. (16)

In this appendix, we derive Eq. (16). Note that the sum over dipole-dipole interactions and the Green function of the transverse electromagnetic field $\mathcal{G}^{\perp}$ give the Green function of the total electromagnetic field $\mathcal{G}$, i.e.,

$$J_{n\lambda,m\mu}+\phi_{n\lambda,m\mu}=\int d^3r\int d^3r'\rho(\mathbf{r}-\mathbf{R}_{n\lambda})\times\rho(\mathbf{r}'-\mathbf{R}_{m\mu})\frac{1}{(2\pi)^3}\times\int d^3q\,\boldsymbol{\mu}\cdot\mathcal{G}(\mathbf{q},\omega)\cdot\boldsymbol{\mu}\times\exp[i\mathbf{q}\cdot(\mathbf{r}-\mathbf{r}')]\ , \tag{A1}$$

with

$$\mathcal{G}(\mathbf{q},\omega)=\frac{4\pi(\omega^2/c^2-\mathbf{qq})}{\omega^2/c^2-q^2+i0}\ . \tag{A2}$$

We then have

$$J_{\lambda\mu}(\mathbf{k})+\phi_{\lambda\mu}(\mathbf{k})=\sum_m[J_{n\lambda,m\mu}+\phi_{n\lambda,m\mu}-\delta_{nm}\delta_{\lambda\mu}(J_{n\lambda n\lambda}+\mathrm{Re}\phi_{n\lambda n\lambda})]\exp[-i\mathbf{k}\cdot(\mathbf{r}_n-\mathbf{r}_m)]$$
$$=\frac{2}{a^2}\sum_{\mathbf{b}}\int dq_z\frac{(\omega/c)^2\mu^2-[\boldsymbol{\mu}\cdot(\mathbf{k}+\mathbf{b}+q_z\hat{z})]^2}{(\omega/c)^2-(\mathbf{k}+\mathbf{b})^2-q_z^2+i0}\exp[iq_z(\lambda-\mu)a]\times\rho(-\mathbf{k}-\mathbf{b})\rho(\mathbf{k}+\mathbf{b})-\delta_{\lambda\mu}(J_{n\lambda n\lambda}+\mathrm{Re}\phi_{n\lambda n\lambda})\ , \tag{A3}$$

where $\mathbf{q}^{\parallel}$ is the projection of $\mathbf{q}$ in the plane, and $\mathbf{b}$ is the reciprocal lattice vector and we have used the relation

$$\sum_m\exp[i(\mathbf{q}-\mathbf{k})\cdot\mathbf{r}_{nm}]=M\sum_{\mathbf{b}}\delta_{\mathbf{q}^{\parallel},\mathbf{k}+\mathbf{b}}\overset{M\to\infty}{\longrightarrow}\frac{(2\pi)^2}{a^2}\sum_{\mathbf{b}}\delta(\mathbf{q}^{\parallel}-\mathbf{k}-\mathbf{b})\ , \tag{A4}$$

where M is the number of lattice points in one layer. Using the following identities,

$$\int dq_z\frac{\exp[iq_z(\lambda-\mu)a]}{(\omega/c)^2-(\mathbf{k}+\mathbf{b})^2-q_z^2+i0}=-i\pi\frac{\exp[i\sqrt{(\omega/c)^2-(\mathbf{k}+\mathbf{b})^2}|\lambda-\mu|a]}{\sqrt{(\omega/c)^2-(\mathbf{k}+\mathbf{b})^2}}\ ,$$

$$\int dq_z\frac{q_z\exp[iq_z(\lambda-\mu)a]}{(\omega/c)^2-(\mathbf{k}+\mathbf{b})^2-q_z^2+i0}=-i\pi\exp[i\sqrt{(\omega/c)^2-(\mathbf{k}+\mathbf{b})^2}|\lambda-\mu|a]\theta(\lambda-\mu)\ ,$$

$$\int dq_z\frac{q_z^2\exp[iq_z(\lambda-\mu)a]}{(\omega/c)^2-(\mathbf{k}+\mathbf{b})^2-q_z^2+i0}=-i\pi\sqrt{(\omega/c)^2-(\mathbf{k}+\mathbf{b})^2}\exp[i\sqrt{(\omega/c)^2-(\mathbf{k}+\mathbf{b})^2}|\lambda-\mu|a]\ ,$$

and carrying out the integration in Eq. (A3), we finally obtain Eq. (16). $\theta(\lambda-\mu)$ was defined in Eq. (17).

APPENDIX B: POLARITON EFFECTS

In this paper we replaced the polariton dispersion relation by the exciton dispersion relation. We now discuss polariton effects. For a monolayer we have from Eqs. (16) and (30)

$$\Gamma(\omega)\simeq\Gamma_1\omega \tag{B1}$$

$$\Gamma_1=\frac{2\pi\mu^2}{a^2c}\left[\frac{1-(\hat{\mu}^{\parallel}\cdot\hat{\kappa}^{\parallel})^2}{\hat{\kappa}_z}-\hat{\mu}_z^2\hat{\kappa}_z\right], \tag{B2}$$

where $\hat{\kappa}=\boldsymbol{\kappa}/\kappa$ and $\hat{\mu}=\boldsymbol{\mu}/\mu$. We have used the fact that $\kappa=\omega/c$ and assume $\rho(\mathbf{k})=1$. Since $\tilde{J}(\mathbf{k},\omega)$ depends weakly on ω, it is a good approximation setting $\tilde{J}(\mathbf{k},\omega)=\tilde{J}(\mathbf{k},\Omega)$. Therefore,

$$S_{\mathrm{LR}}(\omega)\sim\frac{1}{1+\Gamma_1^2}\frac{1}{\{\omega-[\Omega+\tilde{J}(\mathbf{k},\Omega)]/(1+\Gamma_1^2)\}^2+[\Omega+\tilde{J}(\mathbf{k},\Omega)]^2\Gamma_1^2/(1+\Gamma_1^2)^2}. \tag{B3}$$

When $\Gamma_1\ll1$, since $\Omega\gg\tilde{J}(\mathbf{k},\Omega)$, we recover the result in Markov approximation

$$S_{\mathrm{LR}}(\omega)\sim\frac{1}{[\omega-\Omega-\tilde{J}(\mathbf{k},\Omega)]^2+\Gamma^2(\mathbf{k},\Omega)}. \tag{B4}$$

Comparing Eqs. (B3) and (B4) we see that polariton effects shift the resonance frequency and change the radiative width. Since

$$\frac{2\pi\mu^2}{a^2c}=(2\pi^2)\frac{(\mu^2/a^3)}{\hbar\Omega}\frac{a}{\bar{\lambda}}\ll1, \tag{B5}$$

we see from Eq. (B2) that $\Gamma_1\ll1$ except $\hat{\kappa}_z\simeq0$, i.e., polariton effects are important only when the incident wave vector is nearly parallel to the plane.

For multilayers, since the real part of $\phi(\Omega)$ depends only weakly on ω, the Markov approximation [replacing $\phi(\omega)$ by $\phi(\Omega)$ in $G(\omega)$] is valid provided

$$\left.\frac{d\Gamma_{\lambda\mu}(\mathbf{k},\omega)}{d\omega}\right|_{\omega=\Omega}\ll1. \tag{B6}$$

Equation (B6) holds when k is not too close to ω/c, and N is not too large. For example, assuming $\mathbf{k}=0$ and in plane μ,

$$\Gamma_{\lambda\mu}=\frac{2\pi}{a^2}\cos[|\lambda-\mu|a\omega/c](\omega/c)\mu^2. \tag{B7}$$

Therefore, Eq. (B6) holds and polariton effects are negligible as long as

$$\frac{Na}{\bar{\lambda}}\ll\frac{\bar{\lambda}}{a}\frac{1}{(2\pi)^3}\frac{\hbar\Omega}{\mu^2/a^3}, \tag{B8}$$

where $\bar{\lambda}=2\pi/\kappa$ is the optical wavelength. Polariton effects are important only when the incident wave vector is nearly parallel to the plane, or the multilayer thickness is very large so that Eq. (B8) does not hold.

APPENDIX C: THE REFLECTION SIGNAL

In this appendix, we calculate the reflected and transmitted signals, and show that the energy-conservation relation holds to linear order for a monolayer. The transverse part of the scattered field at point $\mathbf{R}$ is

$$\begin{aligned}\mathbf{E}_{\mathrm{sc}}(\mathbf{R},\omega)&=\mathbf{E}e^{i\boldsymbol{\kappa}\cdot\mathbf{R}}-\int d^3r\,\mathcal{G}^{\perp}(\mathbf{R}-\mathbf{r},\omega)\sum_{n\lambda}\cdot\mathbf{P}_{n\lambda}(\omega)\rho(\mathbf{r}-\mathbf{R}_{n\lambda})\\&=\mathbf{E}e^{i\boldsymbol{\kappa}\cdot\mathbf{R}}-\frac{1}{(2\pi)^3}\int d^3q\,\mathcal{G}^{\perp}(\mathbf{q},\omega)\cdot e^{i\mathbf{q}\cdot\mathbf{R}}\rho(\mathbf{q})M\sum_b\delta_{q^{\parallel},\mathbf{k}+\mathbf{b}}\sum_{\lambda=1}^{N}\mathbf{P}_{\lambda}(\mathbf{k},\omega)e^{-iq_z\lambda a}.\end{aligned} \tag{C1}$$

The first term on the right-hand side is the external field, and the second term is the field created by the polarization in the multilayers. Here $\mathbf{b}$ is the reciprocal lattice vector, and we have used Eq. (21a). Substituting Eq. (A4) into Eq. (C1), we get

$$\begin{aligned}E_{\mathrm{sc}}(\mathbf{R},\omega)=Ee^{i\boldsymbol{\kappa}\cdot\mathbf{R}}-\frac{1}{a^2}\sum_b\int dq_z\frac{2(\omega/c)^2}{(\omega/c)^2-(\mathbf{k}+\mathbf{b})^2-q_z^2+i0}\left[1-\frac{(\mathbf{k}+\mathbf{b}+q_z\hat{z})(\mathbf{k}+\mathbf{b}+q_z\hat{z})}{(\mathbf{k}+\mathbf{b})^2+q_z^2}\right]\\\times\rho(\mathbf{k}+\mathbf{b})\exp[i(\mathbf{k}+\mathbf{b}+q_z\hat{z})\cdot\mathbf{R}]\sum_{\lambda=1}^{N}\mathbf{P}_{\lambda}(\mathbf{k},\omega)e^{-iq_z\lambda a}.\end{aligned} \tag{C2}$$

We next perform the integration over q_z. Since the optical wavelength is much longer than the lattice constant a, $|\mathbf{b}|\gg k,\omega/c$ except for $\mathbf{b}=0$. Therefore, the $\mathbf{b}\neq0$ terms give a contribution proportional to $e^{-b|R_z|}$ which decays rapidly for large R_z and can be neglected. The $\mathbf{b}=0$ term gives the two plane-waves result corresponding to the reflected and

transmitted field,

$$\mathbf{E}_{sc}(\mathbf{R},\omega)=\begin{cases}E_t(\omega)e^{i\kappa\cdot\mathbf{R}} & \text{for } R_z>0\\ E_r(\omega)e^{i\kappa'\cdot\mathbf{R}} & \text{for } R_z<0\end{cases}, \tag{C3}$$

where $\kappa'=\mathbf{k}-\kappa_z\hat{z}$, and $E_r(\omega)$ and $E_t(\omega)$ are given in Eqs. (24) and (25). We have assumed $\kappa_z>0$, and used the fact $\kappa=\omega/c$ and $\kappa_z=\sqrt{(\omega/c)^2-k^2}$.

Now we prove the energy conservation to linear order [Eq. (29)] for a monolayer. Substituting Eq. (21b) into Eqs. (24) and (25), we obtain

$$|E_r^{(1)}(\omega)|^2+|E_t^{(1)}(\omega)|^2=|E|^2+\frac{4\pi^2(\omega/c)^4(\boldsymbol{\mu}\cdot\mathbf{E})^2}{a^4\kappa_z^2}|G(\mathbf{k},\omega)|^2[2\mu^2-(\boldsymbol{\mu}\cdot\hat{\kappa})^2-(\boldsymbol{\mu}\cdot\hat{\kappa}')^2]$$
$$\times|\rho(\mathbf{k})\rho(-\mathbf{k})|^2+\frac{4\pi(\omega/c)^2}{a^2\kappa_z}\,\mathrm{Im}G(\mathbf{k},\omega)\rho(\mathbf{k})\rho(-\mathbf{k})(\boldsymbol{\mu}\cdot\mathbf{E})^2 . \tag{C4}$$

We have used the assumption that the external wave is transverse $\mathbf{E}(\omega)\cdot\hat{\kappa}=0$. We next substitute Eq. (15) into this equation, and use the expression (for monolayer)

$$\mathrm{Im}G(\mathbf{k},\omega)=\mathrm{Im}\phi_{\lambda\lambda}(\mathbf{k},\omega)|\mathbf{G}(\mathbf{k},\omega)|^2 , \tag{C5}$$

where $\mathrm{Im}\phi_{\lambda\lambda}(\mathbf{k},\omega)$ is obtained from Eq. (16)

$$\mathrm{Im}\phi_{\lambda\lambda}(\mathbf{k},\omega)=-(2\pi/a^2)\rho(\mathbf{k})\rho(-\mathbf{k})\times\left[\frac{\mu^2(\omega/c)^2-(\boldsymbol{\mu}^{\parallel}\cdot\mathbf{k})^2}{\sqrt{(\omega/c)^2-k^2}}-\mu_z^2\sqrt{(\omega/c)^2-k^2}\right] . \tag{C6}$$

The last two terms on the right-hand side of Eq. (C4) cancel, resulting in Eq. (29).

APPENDIX D: THE REFLECTION SIGNAL FOR NEAREST-NEIGHBOR INTERLAYER INTERACTION

In this appendix, we calculate the linear and the nonlinear reflection signal using the LFA and the approximations given by Eqs. (31) and (32), i.e., neglecting the interaction between planes beyond the nearest neighbor, and assuming that the radiative coupling between planes is independent of distance between planes. From Eqs. (15) and (30) we have

$$\hat{G}=(\omega-\Omega-\tilde{J}+i\Gamma+i\eta)^{-1}$$
$$=G-iG\Gamma G+(-i)^2G\Gamma G\Gamma G+\cdots , \tag{D1}$$

where

$$G=(\omega-\Omega-\tilde{J}+i\eta)^{-1} . \tag{D2}$$

Here $\hat{G},G,\tilde{J},\Gamma$ denote the $N\times N$ matrices $\hat{G}(\mathbf{k},\omega),G(\mathbf{k},\omega),\tilde{J}(\mathbf{k}),\Gamma(\mathbf{k})$. For brevity we have omitted the $\mathbf{k}$ and ω argument. Substituting $\Gamma_{\lambda\mu}=\Gamma$ into Eq. (D1), we have

$$\hat{G}_{\lambda,\mu}=G_{\lambda,\mu}-\frac{i\Gamma G_\lambda G_\mu}{1+i\Gamma G_0} \tag{D3}$$

where

$$G_\lambda=\sum_{\mu=1}^{N}G_{\lambda,\mu}=\sum_{\mu=1}^{N}G_{\mu,\lambda} , \tag{D4}$$

$$G_0=\sum_{\lambda,\mu=1}^{N}G_{\lambda,\mu} . \tag{D5}$$

We then have

$$S_{LR}(\omega)\propto\left|\sum_{\lambda,\mu=1}^{N}\hat{G}_{\lambda\mu}(\mathbf{k}=0,\omega)\right|^2=|G_0/(1+i\Gamma G_0)|^2 . \tag{D6}$$

Since the real symmetric matrix $\tilde{J}$ contains only nearest-neighbor interactions, we can easily find its eigenvalues and eigenvectors, and obtain

$$G_{\lambda,\mu}=\sum_{\alpha=1}^{N}\frac{1}{\omega-\varepsilon_\alpha+i\eta}\psi_\alpha(\lambda)\psi_\alpha^*(\mu) , \tag{D7}$$

with eigenvalues ε_α given by Eq. (34), and eigenvectors

$$\psi_\alpha(\mu)=\left[\frac{2}{N+1}\right]^{1/2}\sin[\alpha\mu\pi/(N+1)] , \quad \mu=1,\ldots,N . \tag{D8}$$

ε_α and $\psi_\alpha(\mu)$ are the exciton energy and eigenfunction in the absence of radiative coupling. Substituting Eqs. (D5) and (D7) into Eq. (D6), we obtain Eq. (33), where ξ_α is proportional to the oscillator strength and is given by Eq. (35).

We next consider the nonlinear reflection signal in the LFA. Substituting Eq. (45) into Eq. (28), we have

$$S_{NR}(\omega)\propto-4(\omega-\Omega)\,\mathrm{Re}\left[\sum_{\mu=1}^{N}\hat{G}_\mu^*\sum_{\lambda=1}^{N}|\hat{G}_\lambda|^2\hat{G}_\lambda^2\right] , \tag{D9}$$

where

$$\hat{G}_\lambda\equiv\sum_{\mu=1}^{N}\hat{G}_{\lambda,\mu} . \tag{D10}$$

We have set $\exp[i\kappa_z a\cdot(\lambda+\mu_1+\mu_2-\mu_3)]=1$ since

$Na \ll \bar{\lambda}$. Substituting Eqs. (D3) and (D7) into Eq. (D10), we have

$$\hat{G}_\lambda = \frac{\sum_{\alpha=1}^{N} \psi_\alpha(\lambda)\sqrt{\xi_\alpha}/(\omega-\varepsilon_\alpha+i\eta)}{\left[1+i\Gamma\sum_{\alpha=1}^{N}\xi_\alpha/(\omega-\varepsilon_\alpha+i\eta)\right]} . \quad \text{(D11)}$$

When ω is close to one of the eigenvalues ε_α, we can write

$$\hat{G}_\lambda \simeq \frac{\psi_\alpha(\lambda)\sqrt{\xi_\alpha}}{\omega-\varepsilon_\alpha+i(\Gamma\xi_\alpha+\eta)} . \quad \text{(D12)}$$

Substituting Eq. (D12) into Eq. (D9), and using the relation

$$\sum_{\lambda=1}^{N} |\psi_\alpha(\lambda)|^4 = (3+\delta_{2\alpha,N+1})/(2N+2) , \quad \text{(D13)}$$

we obtain Eq. (46).

*Also at Department of Physics, University of Rochester, Rochester, New York 14627.

†Also at Institute of Spectroscopy, Russian Academy of Sciences, Troitsk, Moscow reg, 142092, Russia.

[1] *Semiconductors and Semimetals,* edited by R. Dingle (Academic, New York, 1987), Vol. 24.

[2] J. W. Matthews and A. J. Blakeslee, J. Cryst. Growth **27**, 118 (1974).

[3] F. F. So, S. R. Forrest, Y. Q. Shi, and W. H. Steier, Appl. Phys. Lett. **56**, 674 (1990); D.-Y. Zang, Y. Q. Shi, F. F. So, S. R. Forest, and W. H. Steier, *ibid.* **58**, 562 (1991).

[4] H. Hoshi, K. Kohama, S. Fang, and Y. Maruyama, Appl. Phys. Lett. **62**, 3080 (1993).

[5] S. Mukamel, *Principles of Nonlinear Optical Spectroscopy* (Oxford, New York, in press).

[6] M. R. Philpott, Adv. Chem. Phys. **23**, 227 (1973).

[7] M. Pope and C. E. Swenberg, *Electronic Processes in Organic Crystals* (Oxford University Press, New York, 1982).

[8] J. Knoester and S. Mukamel, Phys. Rep. **205**, 1 (1991); O. Dubovsky and S. Mukamel, J. Chem. Phys. **96**, 9201 (1992).

[9] J. Bounds and W. Siebrand, Chem. Phys. Lett. **75**, 414 (1980).

[10] E. A. Silinsh, *Organic Molecular Crystals* (Springer-Verlag, Heidelberg, 1980).

[11] F. F. So and S. R. Forrest, Phys. Rev. Lett. **66**, 2649 (1991).

[12] E. I. Haskal, Y. Zhang, P. E. Burrows, and S. R. Forrest, Chem. Phys. Lett. **219**, 325 (1994).

[13] S. Schmitt-Rink, D. S. Chemla, and D. A. B. Miller, Adv. Phys. **38**, 89 (1989).

[14] H. Haug and S. W. Koch, *Quantum Theory of the Optical and Electronic Properties of Semiconductors* (World Scientific, New Jersey, 1990).

[15] Z. K. Tang, A. Yanase, T. Yasui, Y. Segawa, and K. Cho, Phys. Rev. Lett. **71**, 1431 (1993).

[16] K. E. Schriver, M. Y. Hahn, and R. L. Whetten, Phys. Rev. Lett. **59**, 1906 (1987).

[17] *Proceedings of the 6th International Symposium on Small Particles and Inorganic Clusters* [Z. Phys. D **26** (1993)].

[18] J. Wörmer, M. Joppien, G. Zimmer, and T. Möller, Phys. Rev. Lett. **67**, 2053 (1991).

[19] D. S. Chemla and J. Zyss, *Nonlinear Optical Properties of Organic Molecules and Crytals, Vols. I and II* (Academic, New York, 1987).

[20] F. C. Spano and S. Mukamel, Phys. Rev. Lett. **66**, 1197 (1991).

[21] H. Ishihara and K. Cho, Mol. Cryst. Liq. Cryst. Sci. Technol. **B4**, 81 (1993); Int. J. Nonlinear Opt. Phys. **1**, 287 (1992).

[22] P. J Feibelman, Phys. Rev. B **9**, 5077 (1974); **12**, 806 (1975); **12**, 4282 (1975); Prog. Surf. Sci. **12**, 287 (1982).

[23] O. Keller, Phys. Rev. B **38**, 8401 (1988).

[24] M. Born and E. Wolf, *Principles of Optics* (Pergamon, New York, 1980).

[25] S. I. Pekar, Zh. Eksp. Teor. Fiz. **33**, 1022 (1957) [Sov. Phys. JETP **6**, 785 (1958)]; *Crystal Optics and Additional Light Waves* (Benjamin, New York, 1983).

[26] J. L. Birman, in *Excitons,* edited by E. I. Rashba and M. D. Sturge (North-Holland, Amsterdam, 1982), p. 72.

[27] V. M. Agranovich and V. L. Ginzburg, *Crystal Optics with Spatial Dispersion and Excitons* (Springer, Berlin, 1984).

[28] R. Zeyher, J. L. Birman, and W. Brenig, Phys. Rev. B **6**, 4613 (1972).

[29] A. D'Andrea and R. Del Sole, Phys. Rev. B **25**, 3714 (1982).

[30] A. D'Andrea and R. Del Sole, in *Excitons in Confined Systems,* edited by R. Del Sole, A. D'Andrea, and A. Lapiccirella (Springer, New York, 1987), p. 102.

[31] V. Chernyak and S. Mukamel, J. Chem. Phys. **100**, 2953 (1994); Phys. Rev. B **48**, 2470 (1993).

[32] N. Wang, V. Chernyak, and S. Mukamel, J. Chem. Phys. **100**, 2465 (1994).

[33] J. K. Jenkins and S. Mukamel, J. Chem. Phys. **98**, 7046 (1993).

[34] J. M. Turlet and M. R. Philpott, J. Chem. Phys. **62**, 4260 (1975); M. R. Philpott and J. M. Turlet, *ibid.* **64**, 3852 (1976).

[35] V. M. Agranovich, R. D. Atanasov, and G. F. Bassani, Chem. Phys. Lett. **199**, 621 (1992).

[36] J. Knoester, Phys. Rev. Lett. **68**, 655 (1992).

[37] V. M. Agranovich and V. E. Kravtsov, Solid State Commun. **55**, 85 (1985).

[38] J. M. Turlet, Ph. Kottis, and M. R. Philpott, Adv. Chem. Phys. **54**, 303 (1983).

[39] H. Port, D. Rund, G. J. Small, and V. Yakhot, Chem. Phys. **39**, 175 (1979).

[40] L. Belleguie and S. Mukamel (unpublished).